Turkish Journal of Electrical Engineering & Computer Sciences

http://journals.tubitak.gov.tr/elektrik/

Research Article

Turk J Elec Eng & Comp Sci
(2018) 26: 999 – 1010

doi:10.3906/elk-1706-209

High-speed switched reluctance machine: natural frequency calculation and acoustic noise prediction

Yusuf YAŞA[1,*], **Yılmaz SÖZER**[2], **Muhammet GARİP**[3]

[1]Department of Electrical Engineering, Faculty of Electrical & Electronics, Yıldız Technical University, İstanbul, Turkey

[2]Department of Electrical & Computer Engineering, College of Engineering, University of Akron, Akron, OH, USA

[3]Department of Mechatronics Engineering, Faculty of Mechanics, Yıldız Technical University, İstanbul, Turkey

Received: 17.06.2017 • **Accepted/Published Online:** 24.01.2018 • **Final Version:** 30.03.2018

Abstract: In this study, an analytical model is proposed for natural frequency calculation and acoustic noise prediction for high speed switched reluctance machines. The developed natural frequency model results are compared with the mechanical finite element analysis results in terms of 6 different mode shapes that cause the majority of the acoustic noise in switched reluctance machines. The results show that the analytical results are consistent with the numerical method results with minimum 90% matching. Based on the natural frequency calculation model, a new acoustic noise prediction method is developed that only needs a radial force waveform as an input emerging on stator pole surfaces. The comparison of the developed and the numerical results clearly indicates that the acoustic noise level of the switched reluctance machine can be effectively found during the design process without using time-consuming numerical methods.

Key words: Acoustic noise, natural frequency calculation, switched reluctance machine, vibration

1. Introduction

Switched reluctance motors (SRMs) are known as double saliency, simple [1], cheap, high efficiency, reliable, robust, and fault tolerant electric machine [2–4]. These outstanding features make the SRM the most appropriate solution in some applications like military, space, and domestic applications [5]; aviation and automotive traction applications, i.e. hybrid-electric vehicles [6]; and mining industry, energy storage, and recovery systems [7]. However, because of the double saliency structure and nonsinusoidal airgap field density of the SRM, enormous vibration and acoustic noise occur, which are mainly caused by the electromagnetic source. This circumstance restricts the use of the SRM in a broad range of applications.

The study of noise and vibration has been performed by different research groups since the 1990s. The widely accepted realities show that three types of sources may cause vibration and acoustic noise in electric machines. Firstly, the electromagnetically generated forces on the windings around the stator teeth cause the movement of each tooth toward the tangential direction. Secondly, the magnetostrictive force occurs due to the physical properties of magnetic materials. Thirdly, magnetic excitation of the stator poles generates radial force components that cause ovulation in the stator and the frame, sequentially [8,9]. This ovulation contributes to the vibration above all. Hence, it is widely accepted that vibration in the stator caused by the radial force constitutes the major part of the acoustic noise in most applications [10–12]. Three types of vibration, i.e. axial,

*Correspondence: yasa@yildiz.edu.tr

torsional and radial, can occur in electric machines. Axial vibration is usually ignored in small and medium-sized electric machines; however, it may cause a considerable amount of deformation in large electric machines such as high power turbo-generators and gas turbine generators, where the axial force cannot be ignored. Torsional vibration occurs when the slots are skewed or the poles are salient. On the other hand, the radial vibration is generally the most common type that affects the stator structure [13].

The radial force is generated by the magnetic field density in the airgap, which is not a sinusoidal distributed in the space, as the excitation phase currents carry many harmonics. When one of the emerged radial force harmonics coincides with any of the stator natural frequencies, mechanical resonance will occur in the structure, which causes vibration and the acoustic noise [14]. Investigation of radial force effects on vibration and acoustic noise needs a multidisciplinary approach that should involve electromagnetic and mechanics. Two approaches exist in the literature. The first approach is establishing the mathematical representation of both electromagnetic and mechanical models of the SRM, which is not straightforward as the machine itself contains nonlinearities. The second approach is utilizing finite element analysis (FEA) by modeling the SRM in Multiphysics software packages. Today, developed FEA software packages offer accurate/realistic results by means of technological advancements but they are costly and time-consuming. Moreover, to reach the acoustic noise level, two-step postprocessing operations are needed after electromagnetic analysis. This makes the parametric optimization highly difficult.

This study proposes an analytical approach that will be an alternative to the mechanical FEA. The developed analytical model is integrated into the electromagnetic FEA. In other words, the user only needs to do electromagnetic FEA to obtain emerged radial forces. By entering the radial force data into the proposed model, the acoustic noise level can be reached in a very short time, which will enable a time effective solution by the adaptation of parametric analysis for SRM acoustic noise optimization.

This paper is organized as follows: natural frequencies' calculation and verification with FEA are given in Section 2. Electromagnetic analysis including phase current optimization and radial force calculation are provided in Section 3. The mechanical-acoustic analytical model is presented and the related results are verified with FEA in Section 4. Finally, the results are summarized in the discussion section.

2. Natural frequency calculation

Natural frequencies of the stator are estimated approximately with the following equations. These expressions are derived considering the stator as a single ring. The effects of winding on natural frequencies are ignored. Moreover, calculation of the natural frequencies by taking into account the frame is not straightforward; it needs a double ring-type model. Thus, the frame is ignored as well.

The most important circumferential mode shapes for vibration and acoustic noise aspects are 1, 2, 3, and 4. The cylindrical geometries circumferential-vibrational modes are shown in Figure 1. The longitudinal vibration modes have a relatively limited effect on small electric machine but they become important in medium-sized and large electric machines. As the mode-2 frequency is usually lower, meaning closer to the fundamental frequency than other mode shapes, it becomes the most predominant mode shape in terms of vibration and acoustic noise [15].

Mode-0 is called pulsating vibration mode and can be estimated by

$$F_{m0} = \frac{1}{2\pi R_m}\sqrt{\frac{E}{\rho\Delta}}, \tag{1}$$

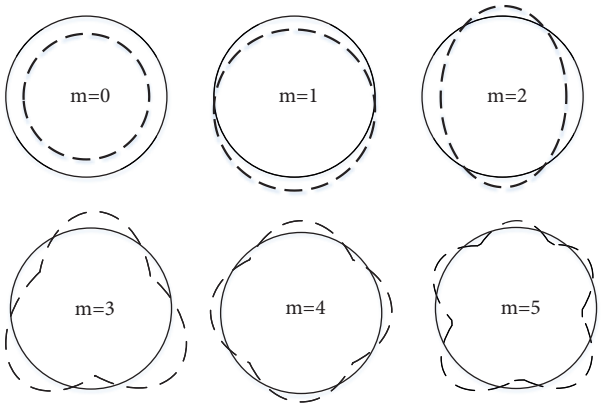

Figure 1. Circumferential vibration mode shapes.

where R_m is the mean yoke radius (Figure 2), E is Young's modulus, ρ is the stator core material density, and $\Delta$is the mass addition factor, which is given by $\Delta = G_s/G_y$. Here G_s and G_y are the stator and the yoke core part total weights, respectively. The first-order mode frequency can be calculated using (2), where h is the yoke thickness and Δ_m is the rotational mass addition factor and can be calculated by (3).

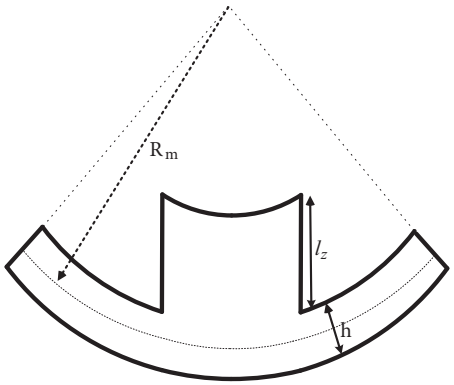

Figure 2. The geometry of the stator structure.

$$F_{m1} = F_{m0}\sqrt{\frac{24R_m^2\Delta}{12R_m^2\Delta + h^2\Delta_m}} \tag{2}$$

$$\Delta_m = 1 + \frac{6N_{stator}\theta_z}{\pi L h^3 R_m} \tag{3}$$

$$\theta_z = A_{tooth}l_{tooth}^3\left(\left(\frac{h}{2l_{tooth}}\right)^2 + \frac{h}{2l_{tooth}} + \frac{1}{3}\right) \tag{4}$$

In the equations, stator slot number, stack length, tooth cross-sectional area, and tooth height are denoted by N_{stator}, L, A_{tooth}, and l_{tooth}, respectively. Any circumferential mode shape equal to or greater than two can be represented by (5).

$$F_{m\geq 2} = \frac{F_{m0} m(m^2-1)}{\sqrt{m^2+1}} \frac{h}{2\sqrt{3}R_m} \frac{1}{\sqrt{\left\{1 + \frac{\frac{1}{12}\frac{h^2}{R_m^2}(m^2-1)\left(m^2\left(4+\frac{\Delta_m}{\Delta}\right)+3\right)}{m^2+1}\right\}}} \tag{5}$$

The given equations are applied to the designed SRM. The related parameters are given in Table 1. The calculated mode shape vibration frequencies and the FEA results are compared in Table 2.

Table 1. Some SRM design parameters.

Parameter	Symbol	Value	Unit
Stator outer radius	R_{out}	38.5	mm
Stator mean radius	R_m	35.5	mm
Stator yoke thickness	h	5.9	mm
Core material density	ρ	7850	kg/m^3
Young modulus	E	$2 \cdot 10^{11}$	N/m^2
Stator weight	G_s	1.08	kg
Stator yoke weight	G_y	0.67	kg
Stator pole number	N_{stator}	6	
Stack length	L	65	mm
Stator pole height	l_{tooth}	12.8	mm

Table 2. Calculated vibration mode natural frequencies of high-speed SRM.

Mode shape	m0	m1	m2	m3	m4	m5
Calculated natural frequency (kHz)	17.84	25.16	2.26	6.17	11.34	17.45
FEA result	16.91	22.82	2.37	5.53	10.81	17.38
Error %	5.21%	9.3%	4.87%	10.53%	4.68%	0.4%

The results show that the calculated and the FEA results match each other over 90%. The FEA result of each mode shape is shown in Figure 3.

3. Electromagnetic analysis

In this section, the electromagnetic analysis of the SRM is performed to figure out the radial forces on each stator tooth surface. The analyses are executed in Ansys-Maxwell finite element software. The electromagnetic analyses are divided into two stages. In the first stage, the analysis is performed in the static case, where one of the phases is excited with the constant current and the generated torque and flux linkages are calculated at different rotor positions. In the static analyses, the torque and flux waveforms are shown in Figure 4. As can be understood in the figure, the SRM works in the linear region at low currents until 15-A current level. However, after 15 A, the SRM reaches the saturation level and the generated electromagnetic torque does not increase proportionally with the current. At 25 A constant phase current, flux lines of the developed SRM for different rotor positions are shown in Figure 5. In the second stage, dynamic analyses are performed where all the phases should be excited with convenient phase current waveforms. To get a proper excitation current waveform, the control parameters, i.e. reference phase current, turn-on angle, and conduction angles, as shown in Figure 6,

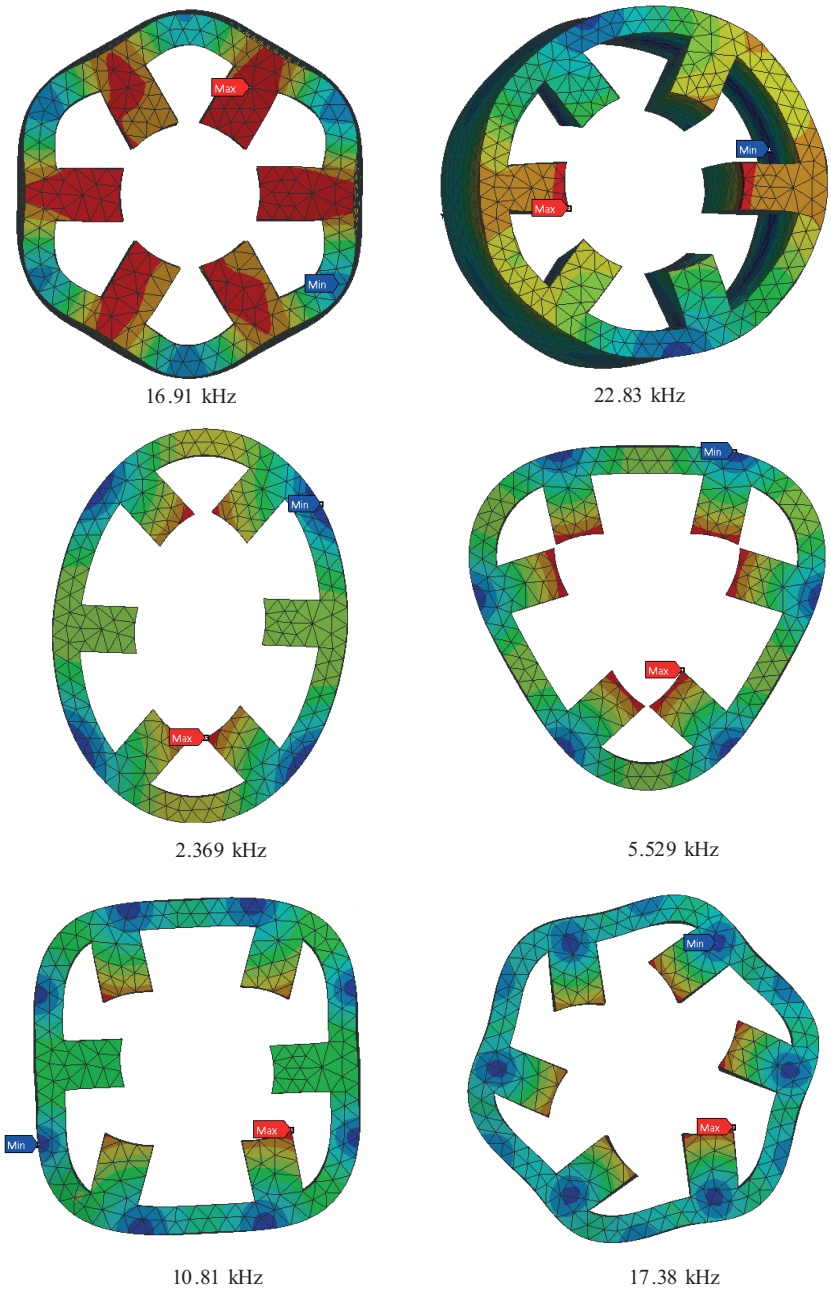

Figure 3. The FEA results of circumferential mode shapes.

are further optimized. The optimization is carried out by modeling the SRM in MATLAB-Simulink. After determining the optimum control parameters, the proper current waveform is applied to the electromagnetic FEA model. Figure 7 shows the torque and the phase currents at 10 krpm operating speed. Fourthly, the radial force that emerges in each stator pole inner surface will be obtained using the following equations, which are derived from the Maxwell stress tensor. These radial forces arising from the electromagnetic excitation of the phases are the main reason for the vibration and acoustic noise in SRMs. Here B_r and B_t are the radial and the tangential components of airgap field density, respectively. μ_0 is the magnetic permeability of free space.

The integration must be operated on the stator pole surface. The resultant radial force waveforms in stator poles are shown in Figure 7c.

$$F_r = \iint \frac{1}{2\mu_0} \nabla B^2 \hat{n} = \frac{1}{2\mu_0} \iint (B_r^2 - B_t^2) dS \tag{6}$$

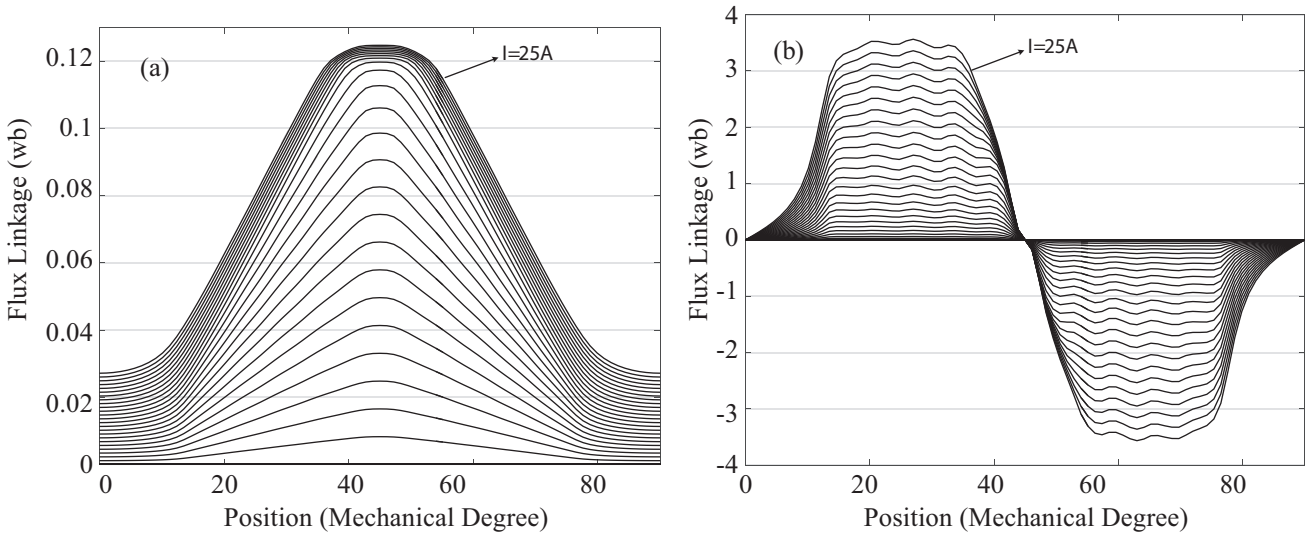

Figure 4. The static flux linkage (a) and torque (b) waveforms of developed SRM.

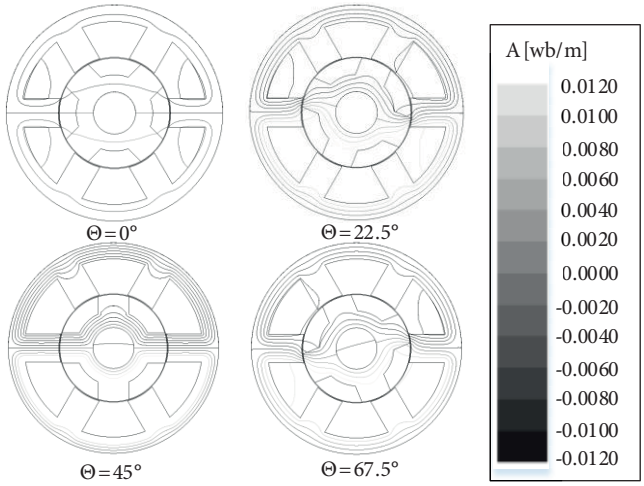

Figure 5. The fluxes of developed SRM for different rotor positions at 25-A excitation current.

4. Mechanical and acoustic noise analysis

In the previous section, the developed SRM's electromagnetic behavior was examined and the radial forces that occur in stator pole surfaces are found. In this section, the mechanical analysis will be performed using the radial forces found. Similar to the natural frequency calculation section, the results will be provided by analytical model and FEA. Finally, both results will be compared to verify the analytical model.

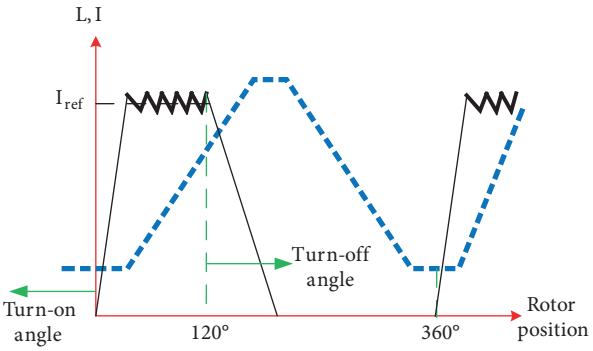

Figure 6. Definition of reference phase current, turn-on, and turn-off angle.

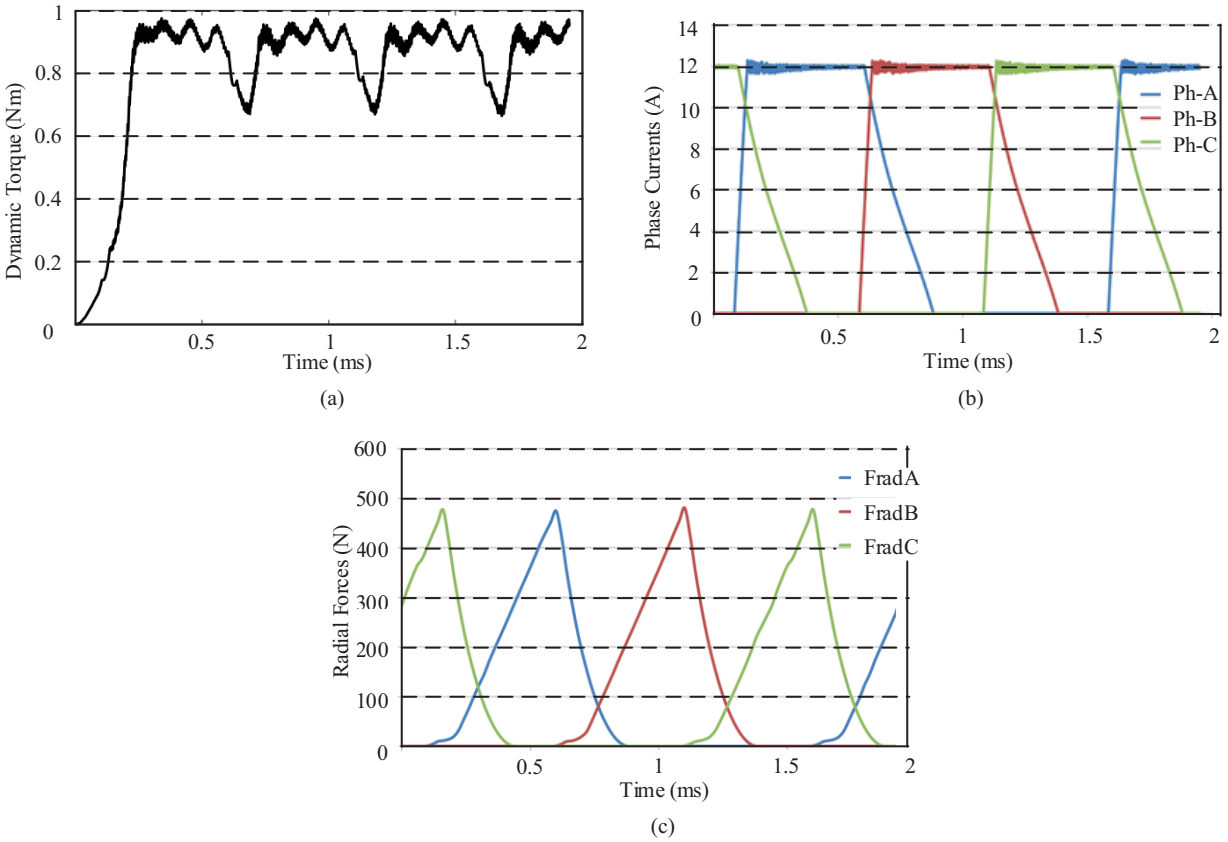

Figure 7. Dynamic torque (a), currents (b), and the radial forces (c) of phases at 10 krpm speed, $I_{ref} = 12A, \theta_{on} = -20^\circ$, and $\theta_{con} = 125^\circ$.

The analytical calculation of the acoustic noise starts with the fast Fourier transform (FFT) of the radial forces. Figure 8 shows the harmonic components of the radial force. The developed SRM is in 6/4 combination. Thus, the fundamental component of the phase current is 666 Hz at 10 krpm speed. As expected, the maximum radial force emerges at the fundamental frequency. As the harmonic order increases, the component magnitudes decrease. If one of the radial force components overlaps with the mentioned natural frequency, the resonance will come out at that frequency. The resonance causes vibration and acoustic noise. Usually, the high magnitude radial force components gather around the fundamental operating frequencies as shown in Figure 8. Therefore,

as the mode-2 natural frequency is close to the fundamental frequency, the maximum acoustic noise will be expected around 2.3 kHz. These force components will be called excitation frequencies (F_{exc}). The vibration on the stator outer surface will generate sound pressure, which is calculated by

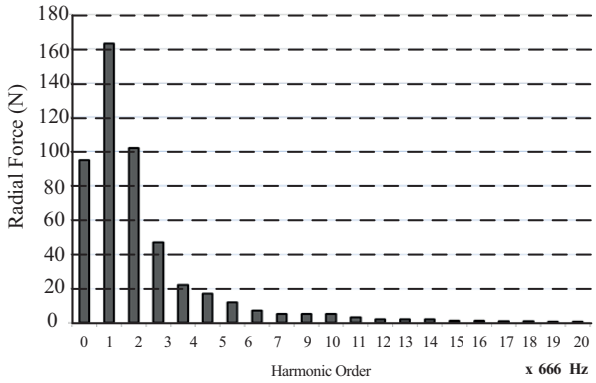

Figure 8. Radial force fast Fourier transform.

$$SP = 10 \log \frac{P}{P_{ref}} \tag{7}$$

Here $P_{ref} = 10^{-12} W$ is the reference sound power and the P is the generated power on the stator outer surface, which is calculated by

$$P = (11.84\pi)^3 \frac{\left(\frac{2\pi R_{out}}{c} F_{exc}\right)}{1 + \left(\frac{2\pi R_{out}}{c} F_{exc}\right)^2} F_{exc}^2 \xi^2 L R_{out} \tag{8}$$

Here c is the speed of sound in the medium and ξ is the total deformation on the stator outer surface, which is calculated by (9), where A_p is the stator pole surface area. In the calculations, the damping effect of the stator is ignored to simplify the equations.

$$\xi = \frac{\frac{12 F_{exc}}{m^4 A_{tooth}} \frac{R_m}{E} \left(\frac{R_m}{h}\right)^3}{1 - \left(\frac{F_{exc}}{F_m}\right)^2} \tag{9}$$

FEA is performed to verify the developed acoustic noise analytical model. The radial force waveforms obtained from the electromagnetic FEA are entered into the mechanical FEA. Stator outer surface acceleration is shown in Figure 9. It is noteworthy to mention that acceleration peaks emerge in natural frequencies 2, 4, and 5. However, mode-3, which is 5.5 kHz, given in Table 2, is damped by the stator structure.

Figure 10 shows the analytical model and FEA acoustic analysis results. As the mode-1 natural frequency is beyond the maximum audible frequency, which is 20 kHz, and mode-0 has limited effect in terms of the airborne noise in small electric machines [14], these two modes are not taken into account in the calculations. The results clearly prove the developed analytical model.

In the last analysis, the mechanical harmonic frequency calculation is performed to see the deformations and the stresses on the machine structure. Figure 11 shows the harmonics analysis results, where the maximum equivalent stress emerges around 3.3 MPa. The stator laminations are made of steel (yield strength for the lamination material used is 370 MPa) and the frame is made of aluminum (yield strength 276 MPa), the

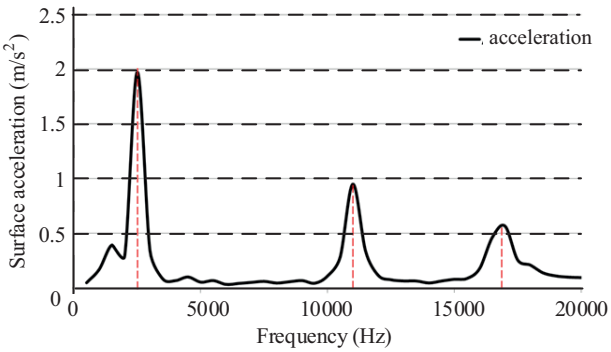

Figure 9. Variation in the SRM stator outer surface acceleration.

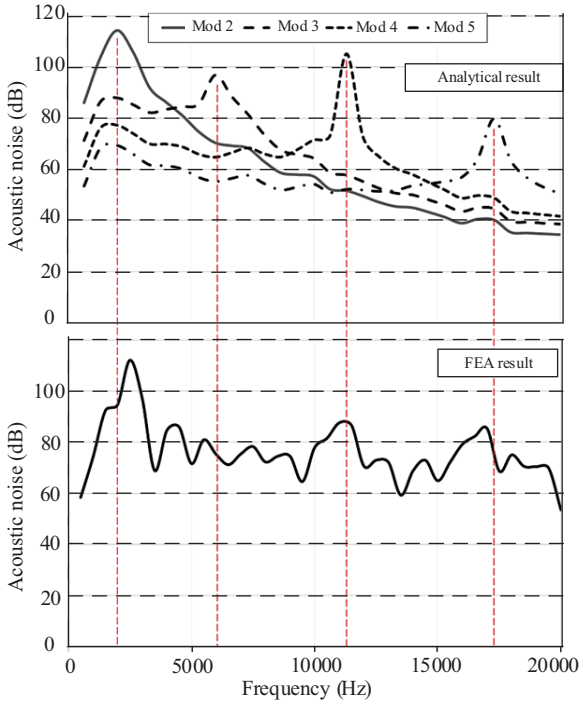

Figure 10. The acoustic noise comparison of analytical and FEA results.

weakest part in the structure is the frame. The results show that the designed geometry has high enough rigidity.

5. Conclusion

The acoustic noise calculation/prediction of any developed SRM in the design stage requires three steps: electromagnetic, mechanical/structural, and acoustic noise analyses. As the acoustic noise is highly affected by both electromagnetic excitations and by machine geometry/structure, the first two steps need to be executed before doing the acoustic calculation. Hence, to reach the acoustic noise level, postprocessing operations are needed, which makes the parametric optimization highly difficult and time-consuming. In this study, a new analytical approach is developed that eliminates time-consuming postprocessing operations (mechanical and

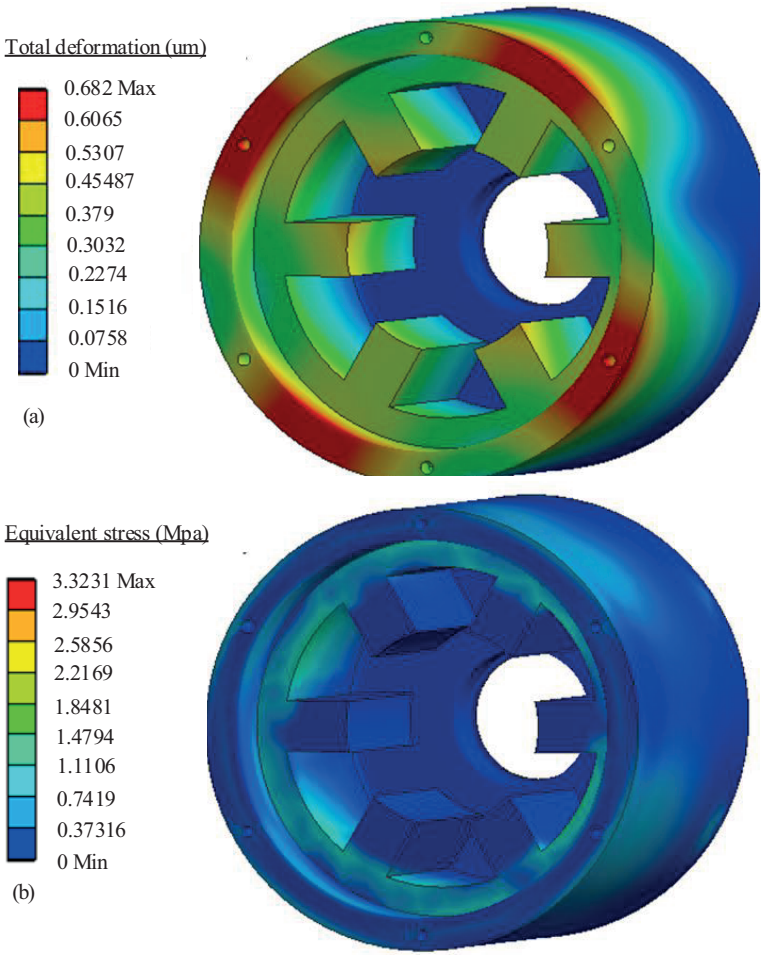

Figure 11. The harmonic analysis results of the developed HS-SRM where the operating conditions are 50 krpm and the output power is 1.8 kW: (a) the maximum deformation, (b) the maximum equivalent stress.

acoustic finite element analyses). The developed analytical acoustic prediction model can be integrated into the electromagnetic FEA. In other words, the user only needs to do electromagnetic FEA to obtain radial forces that emerged on the stator teeth surfaces. Then the force data obtained are entered into the proposed model to get the acoustic noise data. In the present study, the natural frequencies are calculated with the developed model and compared with FEA results. The results are highly consistent with at least 90% overlapping with FEA results. Based on the natural frequency calculation, the acoustic pressure level is obtained in a frequency domain for each modal shape. The results verify the validity of the developed acoustic noise model.

Acknowledgment

This study was supported by the Scientific and Technological Research Council of Turkey (TÜBİTAK). TÜBİTAK is acknowledged for granting Yusuf Yaşa an International Doctoral Research study in the framework of TÜBİTAK-BİDEB 2214 grant.

Nomenclature

E	N/m^2	Elasticity modulus (Young's modulus)
$R_m R_{out}$	m	Mean radius of stator yoke and the stator outer radius
ρ	Kg/m^3	Core material density
$\Delta\Delta_m$		Normal and rotational mass addition factor
G_s, G_y	kg	Stator and yoke weights
h, L, l_{tooth}	m	Yoke thickness, stator stack length, and tooth height
A_{tooth}	m^2	Tooth cross-sectional area
N_{stator}		Stator slot number
m		Mode number
B_r, B_t	T	Radial and the tangential components of airgap field density.
μ_0	N/A^2	Magnetic permeability of free space, which is $4\pi 10^{-7}$.
$F_{m0}\, to\, F_{m5}$	Hz	Natural mode frequencies
P, P_{ref}	W	Sound power and reference sound power
SP	Pa	Sound pressure
c	m/s	The speed of sound in a medium, which is 343.
F_{exc}	Hz	Excitation frequency
ξ	m	Total deformation on the stator outer surface

References

[1] Hua W, Hua H, Xu X, Zhao G, Cheng M. Analysis and experimental validation of a half-teeth-wound switched reluctance machine. IEEE T Magn 2014; 50: 1-5.

[2] Parrang S, Ojeda J, Khelladi S, Gabsi M. Aeroacoustic noise prediction for SRM. In: 7th IET International Conference on Power Electronics, Machines and Drives (PEMD 2014); 8–10 April 2014; Manchester, United Kingdom. Stevenage, United Kingdom: IET. pp. 1-6.

[3] Takeno M, Chiba A, Hoshi N, Ogasawara S, Takemoto M, Rahman MA. Test results and torque improvement of the 50-kw switched reluctance motor designed for hybrid electric vehicles. IEEE T Ind Appl 2012; 48: 1327-1334.

[4] Bilgin B, Emadi A, Krishnamurthy M. Comprehensive evaluation of the dynamic performance of a 6/10 SRM for traction application in PHEVs. IEEE T Ind Electron 2013; 60: 2564-2575.

[5] Wu CY, Pollock C. Analysis and reduction of vibration and acoustic noise in the switched reluctance drive. In: Industry Applications Conference Twenty-Eighth IAS Annual Meeting; 2–8 October 1993; Toronto, Ontario, Canada: IEEE. pp. 91-98.

[6] Yang Z, Shang F, Brown IP, Krishnamurthy M. Comparative study of interior permanent magnet, induction, and switched reluctance motor drives for EV and HEV applications. IEEE Transactions on Transportation Electrification 2015; 1: 245-254.

[7] Michon M, Calverley SD, Atallah K. Operating strategies of switched reluctance machines for exhaust gas energy recovery systems. IEEE T Ind Appl 2012; 48: 1478-1486.

[8] Liang X, Li G, Ojeda J, Gabsi M, Ren Z. Comparative study of classical and mutually coupled switched reluctance motors using multiphysics finite-element modeling. IEEE T Ind Electron 2014; 61: 5066-5074.

[9] Liang XB, Li GJ, Ojeda J, Gabsi M, Ren Z. Comparative study of vibration and acoustic noise between classical and mutually coupled switched reluctance motors. In: 20th International Conference on Electric Machines (ICEM 2012); 2–5 September 2012; Marseille, France. New York, NY, USA: IEEE. pp. 2955-2960.

[10] Fiedler JO, Kasper KA, De Doncker RW. Calculation of the acoustic noise spectrum of SRM using modal superposition. IEEE T Ind Electron 2010; 57: 2939-2945.

[11] Cameron DE, Lang JH, Umans SD. The origin and reduction of acoustic noise in doubly salient variable-reluctance motors. IEEE T Ind Appl 1992; 28: 1250-1255.

[12] Hendershot JR. Causes and sources of audible noise in electric motors. In: 22nd Incremental Motion Control Systems Devices Symposium; 1993; Marseille, France. New York, NY, USA: IEEE. pp. 259-270.

[13] Shin HJ, Choi JY, Cho HW, Jang SM. Analysis on electromagnetic vibration source permanent magnet synchronous motor for compressor of electric vehicles. In: IEEE Vehicle Power and Propulsion Conference; 9–12 October 2012; Seoul, Korea. New York, NY, USA: IEEE. pp. 200-203.

[14] Anwar MN, Husain I. Radial force calculation and acoustic noise prediction in switched reluctance machines. IEEE T Ind Appl 2000; 36: 1589-1597.

[15] Yang SJ. Low-noise Electrical Motors. Oxford, UK: Oxford University Press, 1981.